



## High Riverine CO<sub>2</sub> Outgassing affected by Land Cover Types in the Yellow River Source Region

Mingyang Tian<sup>1</sup>, Xiankun Yang<sup>2</sup>, Lishan Ran<sup>3</sup>, Yuanrong Su<sup>1</sup>, Lingyu Li<sup>1</sup>,

Ruihong Yu<sup>1</sup>, Haizhu Hu<sup>1\*</sup>, Xi Xi Lu<sup>1,4\*</sup>

5 <sup>1</sup>Inner Mongolia key laboratory of river and lake ecology, School of ecology and environment, Inner Mongolia University, Hohhot, 010021, China

<sup>2</sup>School of Geographical Sciences of Guangzhou University, Guangzhou, 510006, China

<sup>3</sup>Department of Geography, The University of Hong Kong, Hong Kong, China

<sup>4</sup>Department of Geography, National University of Singapore, 117570, Singapore

10

✉ *Corresponding author*

Xi Xi Lu Tel.: +86-471-4991469, Fax: +86-471-4991436, e-mail: [geoluxx@nus.edu.sg](mailto:geoluxx@nus.edu.sg)

Haizhu Hu Tel.: +86-471-4991469, Fax: +86-471-4991436, e-mail: [huhaihu@163.com](mailto:huhaihu@163.com)

15



**Abstract:** Rivers connect the land and the oceans, acting as both active pipes and containers transporting carbon and other substances from terrestrial ecosystems to aquatic ecosystems. Meanwhile, rivers can release huge amounts of CO<sub>2</sub> to the atmosphere. However, estimates of global riverine CO<sub>2</sub> emissions remain greatly uncertain owing to the absence of a comprehensive spatially and temporally CO<sub>2</sub> emissions measurement, especially in river source regions. In this study, riverine partial pressure of CO<sub>2</sub> (*p*CO<sub>2</sub>) and CO<sub>2</sub> efflux (*F*CO<sub>2</sub>) in the Yellow River source region under different landcover types, including glaciers, permafrost, wetlands, and grasslands, were investigated in April, June, August, and October 2016. The relevant chemical parameters and environmental parameters, including pH, dissolved oxygen (DO), and dissolved organic carbon (DOC), were analyzed to explore the main control factors of riverine *p*CO<sub>2</sub> and *F*CO<sub>2</sub>. The results showed that the rivers in the Yellow River source region were a net CO<sub>2</sub> source, with the *p*CO<sub>2</sub> ranging from 181 to 2441 μatm and the *F*CO<sub>2</sub> from -221 to 6892 g C m<sup>-2</sup> yr<sup>-1</sup>. Both the *p*CO<sub>2</sub> and *F*CO<sub>2</sub> showed strong spatial and temporal variations. The average *F*CO<sub>2</sub> in August was higher than that in other months, with the lowest in October. In alpine climates, low temperature conditions played a crucial role in limiting biological activity and reducing CO<sub>2</sub> emissions. The lowest *F*CO<sub>2</sub> values (-221 g C m<sup>-2</sup> yr<sup>-1</sup>) were observed in the glacier and permafrost regions. By integrating seasonal changes of water surface area, the total CO<sub>2</sub> efflux was estimated at 0.37±0.49 Tg C yr<sup>-1</sup>, which is significantly higher than previous studies. Although it is still a small proportion of CO<sub>2</sub> emissions compared with the whole Yellow River Basin, but there is a huge carbon emissions potential. Since the permafrost in the source region of the Yellow River is rich in large amounts of ice and organic carbon, the continuously increasing temperature due to global warming will accelerate not only the mobilization of organic carbon in permafrost, but also the degradation of organic carbon by soil microorganisms. As a consequence, huge amounts of CO<sub>2</sub> release from soils and rivers is anticipated.

**Key words:** *p*CO<sub>2</sub>; CO<sub>2</sub> outgassing; glaciers; permafrost; wetland; grassland; Yellow River source region



## 1. Introduction

40 Rivers connect the land and the oceans, acting as both pipes and containers transporting carbon and other substances from terrestrial ecosystems to aquatic ecosystems. At the same time, they receive organic or inorganic carbon from the terrestrial carbon pool, degrade and ultimately release as CO<sub>2</sub> or buried in the riverine sediments. The existing studies on riverine CO<sub>2</sub> evasion mainly focuses on the spatial and temporal dynamics of partial pressure of CO<sub>2</sub> ( $p\text{CO}_2$ ) and CO<sub>2</sub> efflux ( $F\text{CO}_2$ ). (Cole et al., 2001; 45 Aufdenkampe et al., 2011; Raymond et al., 2013; Abril et al., 2014). Many researchers believe that river water CO<sub>2</sub> is mainly derived from the respiration of terrestrial ecosystems and the decomposition of organic matter in river waters, but the source and impact mechanism of CO<sub>2</sub> evolution from rivers is still not clear (Raymond et al., 2013; Hotchkiss et al., 2015; Schelker et al., 2016; Ran et al., 2017). Therefore, in order to accurately estimate the riverine CO<sub>2</sub> outgassing and in-deep understanding its control 50 mechanism, more research within the river in particular climates (i.e., alpine climate) and special regions (i.e., headwater region or intermitted rivers) are needed. It will provide a better understanding of regional or global carbon balance processes and future climate change trends.

With respect to global-scale CO<sub>2</sub> outgassing, available estimates are characterized by great uncertainty. 55 For example, recent CO<sub>2</sub> outgassing fluxes from global rivers and streams combined range from 1.8 to 3.2 P g C yr<sup>-1</sup> (Raymond et al., 2013; Drake et al., 2017), which are significantly higher than earlier estimate by Cole et al. (2007) (i.e., 0.75 P g C yr<sup>-1</sup> based on the data of 80 major rivers in the world). A major reason for the huge range is because of the absence of a global CO<sub>2</sub> outgassing database which includes CO<sub>2</sub> emissions measurement over different rivers and under different climate and land cover 60 types (Raymond et al., 2013; Cole et al., 2007; Aufdenkampe et al., 2011; Drake et al., 2017). Thus, more field measurements based on global river systems are strongly needed to increase the accuracy of the



estimates.

However, there are limited studies on CO<sub>2</sub> effluxes of rivers in extreme geographical and climatic conditions, such as alpine rivers (Wu et al., 2008; Zhang et al., 2013). Crawford et al. (2013) investigated the riverine CO<sub>2</sub> outgassing in the Alaska region and explored its temporal and spatial changes by connecting it to land use types. Crawford et al. (2015) further studied carbon emissions from the rivers and lakes in alpine areas around Estes Park in the United States and found the average  $p\text{CO}_2$  was only 417  $\mu\text{atm}$ . They concluded that the high altitude and low vegetation coverage are the primary factors limiting CO<sub>2</sub> outgassing. Weyhenmeyer et al. (2015) collected data from 5,118 alpine lakes and concluded that the production of CO<sub>2</sub> in the lake was usually half of the CO<sub>2</sub> emissions and most of the emitted CO<sub>2</sub> derived from dissolved inorganic carbon (DIC). Humborg et al. (2010) surveyed rivers in central and northern Sweden and concluded that the average  $p\text{CO}_2$  was 1445  $\mu\text{atm}$  and the average  $F\text{CO}_2$  value was 3033 g C m<sup>-2</sup> yr<sup>-1</sup>. A comprehensive analysis indicated that groundwater and respiration of soil maintained the riverine CO<sub>2</sub> excess with the consumption of terrestrial organic matter as the major source of riverine CO<sub>2</sub>. Overall, compared with the temperate and tropical rivers, riverine CO<sub>2</sub> outgassing under the alpine climate is at a relatively low level. It is mainly due to the cold climate with low temperature and high altitude that limit riverine CO<sub>2</sub> emissions, and the underlying control mechanisms are not the same as these in temperate and tropical climates (Peter et al., 2014).

80

The riverine CO<sub>2</sub> emissions in the Yellow River Basin have been studied and some preliminary results have been reported. Su et al. (2005) reported that the  $p\text{CO}_2$  value of the mainstream was between 1100 and 1700  $\mu\text{atm}$ , which were in the intermediate-low level of the world rivers. The main controlling factor was its carbonate system. Zhang et al. (2008) measured  $p\text{CO}_2$  of 1570  $\mu\text{atm}$  at Lijin Hydrological Station



85 on the lower Yellow River during sediment regulation period (June–July), which was significantly higher  
than in the other periods. Zhang et al. (2009) measured the  $FCO_2$  of the Yellow River and concluded that  
the Yellow River water was a source of atmospheric  $CO_2$  during the autumn. The amount was about  
0.0174 Tg C, and the flux was similar to that of the Ottawa River but far less than that of the Amazon.  
Ran et al. (2015b) estimated that the annual  $CO_2$  emissions of the whole Yellow River at 7.9 Tg C, which  
90 is close to the basin-wide carbon deposition of 8.7 Tg C while larger than the amount of marine import  
(i.e., 6 Tg C).

These studies on  $CO_2$  emissions from the Yellow River were mainly confined to its middle and lower  
reaches and the estuary. In contrast, there are few studies on the upper reaches, especially the source  
95 region on the Tibetan Plateau. The Yellow River source region is located in the alpine zone with the  
Yellow River mainstream and its tributaries flowing through a variety of land cover types, including  
grassland, wetland, glacier, and permafrost. Affected by increasing temperature as a result of global  
warming, the alpine rivers in this region have become hot spots of riverine carbon cycle studies and  
warrant a thorough understanding of their implications in the context of global climate change (Ulseth et  
100 al., 2018; Peter et al., 2014; Hood et al., 2015). In particular, although Ran et al., (2015a,b) used compiled  
water chemistry data to estimate  $pCO_2$  and  $FCO_2$ , there are no field-based direct measurements of  $CO_2$   
emissions from these alpine rivers.

In order to accurately determine the intensity of riverine  $CO_2$  outgassing and fully understand the  
105 underlying control mechanisms in the alpine climate region, we conducted in situ measurements of  $CO_2$   
emissions from the alpine rivers under different land cover types, including grassland, peatland, glacier,  
and permafrost, in the Yellow River source region. Here we aim to address three questions regarding  $CO_2$



emissions in the Yellow River source region: (1) the spatiotemporal patterns of CO<sub>2</sub> emissions under  
different land cover types; (2) the magnitudes of stream CO<sub>2</sub> emissions; and (3) the source of riverine  
110 CO<sub>2</sub> in this alpine river system. Answers to these questions will lead to a better understanding of riverine  
carbon export and CO<sub>2</sub> emissions, especially for alpine rivers, which will help refine the global estimation  
of riverine *F*CO<sub>2</sub>.

## 2. Materials and methods

### 115 2.1 Site description

The Yellow River originates from the north part of the Bayanhar Mountains in the Tibetan Plateau, then  
flows through the Loess Plateau and the North China Plain, and eventually empties into the Bohai Sea.  
Generally, the drainage basin above the Toudaoguai hydrological station is called the upper reach and the  
region above the Tangnaihai hydrological station is known as the Yellow River source region (Figure 1).

120

The study area is situated from 32°3'N 95°5'E to 36°1'N 103°3'E (Figure 1). In the Yellow River source  
region, most of the rivers flow through the Tibetan Plateau at an altitude of 3000–4000 m with  
meandering river channels. The study area is about  $1.32 \times 10^5$  km<sup>2</sup>, accounting for about 17.6 % of the  
Yellow River basin. The Yellow River source region is located in an alpine zone, which is a typical  
125 plateau continental climate, mainly affected by plateau monsoon. The northern part belongs to the semi-  
arid climate zone, while the middle and southern part is in the humid and sub-humid climate zone (Yang  
et al., 1991).

The annual mean precipitation is 486 mm, which is the dominant factor of runoff (Sun et al., 2009),  
130 accounting for approximately 95.9% of the total runoff in the source area (Liu et al., 2005). The annual



evaporation varies from 800 to 1200 mm. Although the area of source region accounts for only 17.6% of the whole basin, it supplies over 33% water of the Yellow River, providing an important water resource for both middle and lower reaches of the Yellow River (Sun et al., 2009). In recent decades, although the precipitation has slightly increased (Chang et al., 2007), the water discharge in the middle and lower reaches has decreased significantly, which has aggravated the water shortage of the downstream region, especially in the non-flood season (Zhang et al., 2012).

## 2.2 Fieldwork and laboratory analysis

In this study, four rounds of field work in April, June, August, and October 2016 were conducted. The riverine  $p\text{CO}_2$  and related environmental factors, including water temperature, pH, dissolved oxygen (DO), were monitored in the field under different land cover types in the Yellow River source region. In total, there are 36 sampling points (Figure 1) within the study area and they can be categorized on the basis of the complexity of river network structure and the land cover types (i.e., glacier, permafrost, wetland, and grassland) (Table 1). In addition, three groundwater samples in grassland covered area were taken to determine its  $p\text{CO}_2$ . The temperature, pH, and DO were measured by using a Multi 3420 analyzer (WTW, Germany) with the accuracies of  $\pm 0.2$  °C,  $\pm 0.004$ , and  $\pm 1.5\%$ , respectively. Before the measurement, the pH probe was calibrated by three pH buffers (e.g., pH 4.01, pH 7.00, and pH 10.01, respectively).

The prior study suggested that, when the pH ranges from 7 to 10,  $\text{HCO}_3^-$  represents 96% of alkalinity, alkalinity can be used to calculate DIC (Hunt et al., 2011). Alkalinity was determined by on-site titration. The collected water sample was subjected to low-pressure suction filtration through a glass fiber filter (Whatman GF/F) with a pore diameter of 0.7  $\mu\text{m}$ . The fiber filter was pre-fired in a muffle furnace at



450 °C. For each water sample, the alkalinity was titrated with 0.1 mol L<sup>-1</sup> HCl within 12 hours after  
155 sampling. Each titration was repeated three times to assure the analytical error below 3%. The Methyl  
orange indicator was used to determine the endpoint of the reaction at pH=4.5. Another 100 mL of the  
filtered water sample was transferred into the specific bottle, added with nitric acid, and preserved in  
refrigerator at 4 °C condition for dissolved organic carbon (DOC) measurement in laboratory. DOC was  
analyzed with the Vario total nitrogen/organic carbon analyzer (Elementar, German), which has a  
160 precision less than 3%.

### 2.3 Calculation of CO<sub>2</sub> emission

In this study, *FCO*<sub>2</sub> was measured by the floating chamber method (Ran et al.,2017) connected with a  
Li-7000 CO<sub>2</sub>/H<sub>2</sub>O analyzer (Li-Cor, Inc, USA). The Li-7000 instrument was calibrated with standard  
165 CO<sub>2</sub> gases of 500 ppm and 2000 ppm before each measurement.

The volume of rectangular floating chamber is 17.8 L and the covered water area is 0.09 m<sup>2</sup>. The chamber  
walls were lowered 3 cm into the water and mounted with plastic foams that had streamlined ends to  
limit artificial disruptions to near-surface turbulence. The chamber is covered with tin foil to reduce the  
170 influence of sun light's heating. The temperature inside the chamber was measured with a waterproof  
thermometer. At the beginning of each experiment, the chamber was placed in the air near the monitoring  
point and the air inside the chamber was continuously circulated in a closed loop that was connected to  
an infrared Li-7000 gas analyzer through rubber-polymer tubes for CO<sub>2</sub> analysis. The instrument  
automatically records the air CO<sub>2</sub> concentration and ambient atmospheric pressure. When the chamber  
175 was placed on the water surface, the analyzer recorded the CO<sub>2</sub> concentration every 2 seconds, and each  
measurement lasted for 6–10 mins. In large rivers with relatively favorable flow conditions, we fixed the



chamber on a small rubber boat and drifted along the water to measure the  $FCO_2$ . In contrast, we used the static chamber method to measurement the  $FCO_2$  in the small rivers or streams which could lead an overestimate of  $CO_2$  evasion to some extent. (Lorke et al., 2015).

180

The  $CO_2$  flux from water is calculated using the following equation (Frankignoulle et al., 1988):

$$FCO_2 = 1000 \times (dpCO_2/dt) (V/RTS) \quad (1)$$

where,  $dpCO_2/dt$  is the slope of  $CO_2$  change within the chamber ( $Pa\ d^{-1}$ ; converted from  $\mu atm\ min^{-1}$ ),  $V$  is the chamber volume (17.8 L),  $R$  is the gas constant,  $T$  is chamber temperature (K), and  $S$  is the area of the chamber covering the water surface ( $0.09\ m^2$ ).

185

Conventionally,  $FCO_2$  can also be estimated from the following equation.

$$FCO_2 = k \cdot K_H \cdot \Delta pCO_2 \quad (2)$$

Where,  $k$  is gas transfer velocity ( $cm\ h^{-1}$ ),  $K_H$  is the Henry's constant for  $CO_2$  at a given temperature, the  $FCO_2$  is the in situ measured riverine  $CO_2$  efflux, and the  $\Delta pCO_2$  is the difference between the surface water and the atmosphere. Using the field-measured  $pCO_2$  in surface water and air,  $k$  can be computed by rearranging Equation (2). In order to facility compare our  $k$  with the results of other studies, we standardized it to a Schmidt number of 600 ( $k_{600}$ ) by assigning the Schmidt number exponent value of 0.5 (Jähne et al., 1987).

190

195 Surface water  $pCO_2$  was calculated using a headspace equilibrium method (Ran et al., 2017). By using an 1100 mL conical flask, 800 mL of water were collected in the depth of 10 cm below the water surface and the remaining volume of 300 mL was filled with ambient air. The flask was immediately closed with a lid and vigorously shaken for 1 min to equilibrate the gas in water and air. The equilibrated gas was



200 automatically injected into the calibrated Li-7000 gas analyzer. The measurements at each site were repeated 3 times and the average was calculated (analytical error below 3%). Surface water  $p\text{CO}_2$  was calculated based on the equations from Dickson et al. (2007):

$$p\text{CO}_2^{\text{water},i} \approx p\text{CO}_2^{\text{headspace},f} + \frac{V_h}{V_w} (p\text{CO}_2^{\text{headspace},f} - p\text{CO}_2^{\text{headspace},i}) / (K_0 RT)$$

Where, the superscripts  $i$  and  $f$  represent initial and final  $p\text{CO}_2$  ( $\mu\text{atm}$ ),  $V_h$  and  $V_w$  are the headspace volume and water volume, respectively,  $K_0$  is the solubility of  $\text{CO}_2$  in water calculated on the basis of 205 solubility constants for  $\text{CO}_2$  from *Weiss* (1974),  $R$  is the universal gas constant ( $8.314 \text{ J mol}^{-1} \text{ K}^{-1}$ ), and  $T$  is the water temperature on Kelvin scale (K). Temperature in the flask after equilibration was measured to correct for changes in temperature compared to in-situ water. The initial  $p\text{CO}_2$  was taken as the  $\text{CO}_2$  concentration in ambient air before the headspace equilibration measurement.

## 210 3.Results

### 3.1 Characteristics of hydro-chemical variables

Water temperature ( $T_w$ ) varied from 0.1 to 27.7 °C with an average of  $11.9 \pm 5.7$  °C. Average  $T_w$  in June ( $15.1 \pm 3.5$  °C) and August ( $17.0 \pm 5.4$  °C) is significantly higher than that in April ( $8.4 \pm 3.8$  °C) and October ( $7.3 \pm 2.4$  °C). Seasonal  $T_w$  difference was more significant at the wetland ( $14.4 \pm 6.4$  °C) and 215 grassland ( $12.5 \pm 5.4$  °C) sites than that in the glacier ( $7.5 \pm 4.1$  °C) and permafrost ( $10.0 \pm 4.0$  °C) sites. These results were expected as the water temperature depends mainly on the air temperature. Spatial variability of the air temperature was consistent with that of the water temperature at almost all the sites, although in some case it was as high as 33 °C. The annual average air temperature in the study area was  $16.7 \pm 6.3$  °C.

220

Water pH ranged from 7.0 to 9.0 with an average of  $7.9 \pm 0.6$  (Table 1). Mean pH based on all the stream



225 samples was  $8.3 \pm 0.4$ ,  $8.6 \pm 0.4$ ,  $7.2 \pm 0.2$ , and  $7.5 \pm 0.4$  in April, June, August, and October, respectively. A slight decreasing trend is observed with the different land cover types in the order of permafrost > glaciers > grassland > wetland, with the average pH value at  $8.1 \pm 0.9$ ,  $7.93 \pm 0.55$ ,  $7.85 \pm 0.59$ , and  $7.7 \pm 0.5$ , respectively (Table 1). Alkalinity ranged from 600 to 7600  $\mu\text{mol L}^{-1}$  with an average  $2871 \pm 1381 \mu\text{mol L}^{-1}$  (Table 1). Alkalinity was higher in the cold months ( $3378 \mu\text{mol L}^{-1}$  in April and  $2941 \mu\text{mol L}^{-1}$  in October) than in the warm months ( $2644 \mu\text{mol L}^{-1}$  in June and  $2326 \mu\text{mol L}^{-1}$  in August). Alkalinity of the river water in glaciers covered area showed consistently the lowest level throughout the year (Table 1), due to the low coverage of carbonate rocks.

230

DO values ranged from  $2.7 \text{ mg L}^{-1}$  to  $12.1 \text{ mg L}^{-1}$  and the basin-wide mean DO was  $7.8 \pm 0.6 \text{ mg L}^{-1}$  in April,  $7.1 \pm 1.4 \text{ mg L}^{-1}$  in June,  $6.7 \pm 0.7 \text{ mg L}^{-1}$  in August and  $7.7 \pm 0.7 \text{ mg L}^{-1}$  in October, respectively (Table 1). For the land cover types, the highest level of DO were in the glacier, with the annual average of  $7.6 \pm 0.8 \text{ mg L}^{-1}$ , followed by the permafrost with  $7.4 \pm 1.4 \text{ mg L}^{-1}$ , the grassland with  $7.3 \pm 0.9 \text{ mg L}^{-1}$ , and peatland with  $7.2 \pm 1.1 \text{ mg L}^{-1}$ , respectively (Table 1).

235

DOC ranged from 0.2 to  $12.2 \text{ mg L}^{-1}$  with an average of  $4.7 \pm 2.7 \text{ mg L}^{-1}$  (Table 1). DOC exhibited strong seasonality across the rivers. The highest DOC concentration occurred in April ( $5.0 \pm 1.6 \text{ mg L}^{-1}$ ), followed by in August ( $4.9 \pm 3.6 \text{ mg L}^{-1}$ ) and June ( $4.7 \pm 2.9 \text{ mg L}^{-1}$ ), and the lowest was found in October ( $4.0 \pm 2.2 \text{ mg L}^{-1}$ ). For the land cover types, the highest level of DOC was in the peatland covered area, with the annual average of  $5.1 \pm 3.7 \text{ mg L}^{-1}$ , followed by the permafrost with  $4.9 \pm 2.4 \text{ mg L}^{-1}$ , the grassland with  $4.6 \pm 2.3 \text{ mg L}^{-1}$ , and the glaciers with  $3.4 \pm 1.1 \text{ mg L}^{-1}$ , respectively (Table 1).

240

We used the measured flow velocity and channel slope to predict the  $k_{600}$  based on the Model 5 presented



245 by Raymond et al. (2012). The computed  $k_{600}$  showed strong statistically significant but weak agreement  
with the model results (Figure 2a). Given the chamber's dampening effect of wind (Matthews et al.,  
2003), there was not any statistically significant relationship between wind and  $k_{600}$  for streams. Instead,  
flow velocity is a relatively good predictor variable of  $k_{600}$  and can approximately explain 15% of its  
variability (Figure 2b). Although we deployed the floating chamber very carefully, but the whole  
250 statistical analysis could not reflect the multi interaction of variety environment factors beyond different  
land cover types through our 36 sampling sites. Additionally, in some sampling points, the Model 5  
overestimated some  $k_{600}$  values especially in some mountainous rivers, mainly due to the water  
temperature played a crucial role in limiting CO<sub>2</sub> transfer between the air-water interface in the plateau  
region although the higher channel slope supported enough condition for water turbulence (Battin et al.,  
255 2008).

### 3.2 Spatial and temporal variations of $p\text{CO}_2$

The  $p\text{CO}_2$  ranged from 181 to 2441  $\mu\text{atm}$  with an average of  $774\pm 377$   $\mu\text{atm}$ , nearly twofold the ambient  
air  $p\text{CO}_2$ . To better illustrate the spatial variability  $p\text{CO}_2$ , Figure 3a, 4a, and 3c showed its changes with  
260 land cover types. The highest average  $p\text{CO}_2$  value appeared in the peatland covered area ( $937\pm 466$   $\mu\text{atm}$ ),  
followed by grassland ( $818\pm 394$   $\mu\text{atm}$ ), glacier ( $645\pm 253$   $\mu\text{atm}$ ), and the permafrost ( $600\pm 212$   $\mu\text{atm}$ ).

The  $p\text{CO}_2$  value showed different temporal variation characteristics for the four land cover types (Figure  
3a, 4a, and 4c). In grassland covered area, the average river  $p\text{CO}_2$  value in April, June, August, and  
265 October was  $836\pm 258$   $\mu\text{atm}$ ,  $609\pm 297$   $\mu\text{atm}$ ,  $1086\pm 551$   $\mu\text{atm}$ , and  $734\pm 253$   $\mu\text{atm}$ , respectively. In  
peatland covered area, the average river  $p\text{CO}_2$  value of April, June, August and October was  $875\pm 436$   
 $\mu\text{atm}$ ,  $792\pm 436$   $\mu\text{atm}$ ,  $1156\pm 630$   $\mu\text{atm}$  and  $926\pm 285$   $\mu\text{atm}$ , respectively. The water  $p\text{CO}_2$  in these two land



cover types showed the same temporal variation pattern, with the highest  $p\text{CO}_2$  occurred in August and the lowest in June for all the land cover types.

270

Unlike in the peatland and grassland regions, the riverine  $p\text{CO}_2$  in the glacier and permafrost regions showed relatively small variations, but still had the similar seasonal variation trends. In the glacier covered area, the average river  $p\text{CO}_2$  value of April, June, August and October was  $635\pm 122 \mu\text{atm}$ ,  $506\pm 31 \mu\text{atm}$ ,  $738\pm 449 \mu\text{atm}$ , and  $632\pm 132 \mu\text{atm}$  respectively. In the permafrost covered area, the average river  $p\text{CO}_2$  value of April, June, August, and October was  $465\pm 216 \mu\text{atm}$ ,  $586\pm 227 \mu\text{atm}$ ,  $591\pm 74 \mu\text{atm}$ , and  $756\pm 231 \mu\text{atm}$ , respectively.

275

### 3.3 Spatial and temporal variations of $FCO_2$

$\text{CO}_2$  emissions exhibited significant spatial and seasonal variations among the 36 stream sites (Table 1, Figure 3b, 4b, and 4d). The  $\text{CO}_2$  effluxes ranged from  $-221$  to  $1469 \text{ g C m}^{-2} \text{ yr}^{-1}$  in April,  $-144$  to  $6892 \text{ g C m}^{-2} \text{ yr}^{-1}$  in August, and  $-34$  to  $2321 \text{ g C m}^{-2} \text{ yr}^{-1}$  in October. While the highest  $FCO_2$  was measured at the wetland covered sites (Site Pt 3 in August,  $6892 \text{ g C m}^{-2} \text{ yr}^{-1}$ ), the lowest  $FCO_2$  was observed at permafrost covered sites (Site Pm 3 in April,  $-221 \text{ g C m}^{-2} \text{ yr}^{-1}$ ) (Table 1). The averaged  $FCO_2$  of all sites was  $479\pm 436$ ,  $261\pm 205$ ,  $873\pm 1220$ , and  $714\pm 633 \text{ g C m}^{-2} \text{ yr}^{-1}$  in April, June, August, and October, respectively. Clearly, rivers in the Yellow River source region were net carbon sources for the atmosphere, despite the great  $FCO_2$  variations over space and time. Grouped by land cover types, the mean  $\text{CO}_2$  efflux shows a significant decreasing trend from wetland ( $767\pm 1644 \text{ g C m}^{-2} \text{ yr}^{-1}$ ), grassland ( $679\pm 610 \text{ g C m}^{-2} \text{ yr}^{-1}$ ), glacier ( $508\pm 588 \text{ g C m}^{-2} \text{ yr}^{-1}$ ) to permafrost ( $302\pm 349 \text{ g C m}^{-2} \text{ yr}^{-1}$ ). Because the intensity of  $FCO_2$  depends on  $p\text{CO}_2$  in stream water, the  $FCO_2$  showed a similar spatial and temporal pattern to the  $p\text{CO}_2$ , although the highest and lowest  $p\text{CO}_2$  and  $FCO_2$  value were not found at the same sampling sites.

285

290



#### 4. Discussion

##### 4.1 Impact of land cover types on riverine $p\text{CO}_2$ and $\text{CO}_2$ outgassing

Among all land cover types, the lowest  $FCO_2$  appeared in the permafrost covered region, with the annual average  $FCO_2$  of  $302 \pm 349 \text{ g C m}^{-2} \text{ yr}^{-1}$ . It is well known that the riverine  $\text{CO}_2$  is derived from land (Dinsmore and Billett., 2013; Hope et al., 2004), and the area covered by permafrost has a high density of organic carbon in soil (Zeng et al., 2004), these soil organic carbons can support large quantities of DOC to the rivers and cause enormous riverine  $\text{CO}_2$  outgassing. The correlation analysis between various hydro-chemical parameters and  $p\text{CO}_2$  in the permafrost region showed that alkalinity, DO were not highly correlated with  $p\text{CO}_2$  and pH, DOC indeed had a close relation with  $p\text{CO}_2$  (Figure 5). The negative relationship between  $p\text{CO}_2$  and pH is explained as dissolved  $\text{CO}_2$  acts as an acid in water (Stumm and Morgan., 1996), and in poorly buffered systems,  $\text{CO}_2$  can be a strong control on the stream pH (Neal et al., 1998; Waldron et al., 2007). This positive correlation between DOC and  $p\text{CO}_2$  suggests the terrestrial related DOC might support partial riverine  $\text{CO}_2$  concentration (Liu et al., 2016). This indicates that DOC is one of the important sources of permafrost river  $\text{CO}_2$ . The DOC concentration in the rivers in the permafrost covered area is relatively high, averaging at  $5.0 \pm 2.4 \text{ mg L}^{-1}$ , which exceeded  $3.6 \pm 1.1 \text{ mg L}^{-1}$  in glacier areas and  $4.6 \pm 2.3 \text{ mg L}^{-1}$  in grasslands, but was close to  $5.1 \pm 3.7 \text{ mg L}^{-1}$  in peatlands, and sometimes even exceeded the DOC concentration of rivers in the peatland covered region. Additionally, the average alkalinity concentration in that region is the highest among four types. However, the  $p\text{CO}_2$  and  $FCO_2$  value in this region were always the lowest during the four campaigns. This was due to the area covered by permafrost usually with the highest elevation and the lowest average temperature among the four types of land cover with the average water temperature around  $9.99 \text{ }^\circ\text{C}$ . These conditions limited the soil respiration and riverine organic matter degradation (Battin et al., 2008). Additionally, in terms of



gas diffusion, although there is sufficient dissolved  $\text{CO}_2$  in the river water, it is not easy for  $\text{CO}_2$  emission  
315 from rivers to the atmosphere in the condition of low temperature and low flow velocity (average:  $0.8 \pm 0.5$   
 $\text{m s}^{-1}$ ) (Alin et al., 2014). In summary, the lower temperature is the main cause of high riverine DOC  
concentrations and low  $\text{CO}_2$  outgassing rate in the permafrost covered region.

The glaciers covered region has the similar temperatures and elevations to the permafrost, thus its  $p\text{CO}_2$   
320 and  $F\text{CO}_2$  values were also lower in the permafrost covered region, with the average value only at  
 $657 \pm 240 \text{ g C m}^{-2} \text{ yr}^{-1}$ . This is probably because all the sampling sites are located on the 1–2 order streams  
characterized by strong hydrologic connection with the terrestrial landscape (Sorribas et al., 2017; Smits  
et al., 2017), and the surrounded environment lack of exogenous terrestrial carbon support. For the glacier  
area, only DOC was related to  $p\text{CO}_2$  (Figure 6d,  $r^2=0.56$ ,  $p < 0.001$ ). The sampling points under the  
325 glaciers are mainly located around the Aemye Ma-chhen Range. Some glacial sampling sites all have  
some ice and snow melting water supply. The glacial-covered river water has the lowest DOC  
concentration with a lowest value of four land cover types ( $3.6 \pm 1.1 \text{ mg L}^{-1}$ ). The area around the Aemye  
Ma-chhen Range without enough vegetation coverage because of the harsh environment of high elevation  
and low annual average water temperature, limiting the DOC source. Poor soil, short water retention, and  
330 low precipitation are the main reason of the low vegetation coverage in this region (Lu et al., 2001). The  
river near the sampling sites of the snow mountain has been cut deep into the B horizon of soils as a  
result of glacial erosion and retreat. Almost all glacial sampling sites are covered with gravel, limiting  
the supply of terrestrial organic carbon to river carbon pools. As a result, the measured DOC  
concentrations in most glacial areas were very low. In glacial rivers, if there is no external supply of DOC,  
335 the whole water DOC contribution only amounted to  $0.34 \mu\text{mol L}^{-1} \text{ CO}_2$  gain. This highlight that the  $\text{CO}_2$   
produced by DOC degradation in the glacial river cannot maintain such a high  $\text{CO}_2$  outgassing rate.



340 Although there is low content of carbon in ice and snow of that region (Wu et al., 2008), the meltwater of ice and snow continues to erode the surrounding bedrock during long-distance transport, resulting in more limestone in the rivers. Previous studies have shown that glaciers contain large amounts of CO<sub>2</sub> (Meese et al., 1997) and DOC (Hood et al., 2009; Singer et al., 2012), which are important sources of CO<sub>2</sub> in glacier rivers. Our observations found that with the increasing distance from the Aemye Marchen Range, the riverine *p*CO<sub>2</sub> exhibited a decrease trend, which could be explained by the dilution effect of water snow-melting water *p*CO<sub>2</sub>. Therefore, the CO<sub>2</sub> in the region is highly likely to be explained by the CO<sub>2</sub> storage from glacier. As the glaciers melt, CO<sub>2</sub> in the glaciers was brought into the river.

345

The river *F*CO<sub>2</sub> is the highest in the peatland coverage area among the 4 studied types. The relation showed that only pH has a negative linear relationship and alkalinity have a weak linear relationship with the *p*CO<sub>2</sub> (Figure 7). In the peatland rivers, the terrestrial-related organic carbon is an important source of riverine CO<sub>2</sub> (Abril et al., 2014; Müller et al., 2015; Billett et al., 2015; Huet et al., 2015). There are many sources of DOC in the peatland. First, the soil in the wetland ecosystem is rich in peat soil. The amount of peat stock in Zoige Peatland is estimated to be 1.9 billion tons, which accounts for about 40% of China's marsh wetland carbon storage (Wang et al., 2012). These carbon supplies to river carbon pools are an important driver for the high *F*CO<sub>2</sub> in the wetlands rivers. On the other hand, soil pore water enriched with high concentrations of dissolved CO<sub>2</sub> continues to enter river waters, and it also provides sufficient carbon sources for rivers (Butman et al., 2011). In addition, the vegetation in the peatland region can also import large amounts of CO<sub>2</sub> into the river water through two other mechanisms. First, vegetation litter and root exudates release unstable organic carbon into the water. These organic carbons are being further decomposed and served as a carbon source for heterotrophic microorganisms. During this process, heterotrophic organisms release CO<sub>2</sub> into water (Abril et al., 2014). On the other hand, the

355



360 respiration of plant roots and soil microorganisms that are submerged in wetland soils releases CO<sub>2</sub>  
directly into the water (Abril et al., 2014). The combined effects of these factors have resulted in rivers  
with high DOC and high *F*CO<sub>2</sub> value in wetlands.

The average *F*CO<sub>2</sub> in the grassland-covered rivers of 818±394 g C m<sup>-2</sup> yr<sup>-1</sup> is at a moderate level, below  
365 the wetland *F*CO<sub>2</sub> but significantly higher than the riverine *F*CO<sub>2</sub> in the glaciers and permafrost covered  
regions. Correlation analysis between water chemistry parameters and riverine *p*CO<sub>2</sub> in this area showed  
that both pH and DOC had weak correlation with *p*CO<sub>2</sub> (Figure 8). This also shows that the pH of river  
water in the area is partial affected by the CO<sub>2</sub> concentration in water. Due to the temperate environment,  
grassland is the most human-affected area in the study area, mainly in the form of grazing. As a result,  
370 beside the DOC derived from the physical erosion, the pollutants produced by grazing are also important  
sources of riverine DOC. The average *p*CO<sub>2</sub> in peatland is 15% higher, but the average DOC  
concentration in wetlands is 11% higher than that in grassland, and the alkalinity in grassland is 46%  
higher than that in wetlands. Therefore, DIC is an important source of riverine CO<sub>2</sub> in grasslands. While  
stream DIC source are highly variable across space and time (Smits et al., 2017), the DIC mainly  
375 originated from groundwater (Marx et al., 2017). Although groundwater is participated in the carbon  
cycle of the river in the entire study area, it is higher in the grassland than in other regions, indicating  
that the supplemental effect of groundwater on the river CO<sub>2</sub> in the grassland is the biggest. We also take  
three groundwater samples in grassland covered area. The average *p*CO<sub>2</sub> of groundwater samples in  
grassland-covered areas is 1976 µatm, which is 2.5 times the average value of the water in the Yellow  
380 River source region. Therefore, in the grass-covered areas, the CO<sub>2</sub> excess in the rivers is maintained by  
both the terrestrial vegetation organic carbon and the inorganic carbon in the groundwater.



#### 4.2 Significance and implications for riverine carbon budgets

The annual average  $p\text{CO}_2$  is  $771 \pm 380 \mu\text{atm}$  and  $F\text{CO}_2$  is  $590 \pm 766 \text{ g C m}^{-2} \text{ yr}^{-1}$  in the Yellow River source  
385 region. In the whole Yellow basin, Ran et al. (2015a, b) estimated the a significantly lower  $p\text{CO}_2$  value  
of  $241 \pm 79 \mu\text{atm}$  and the areal  $\text{CO}_2$  efflux of this region is  $-221 \pm 112 \text{ g C m}^2 \text{ yr}^{-1}$ , indicative of a strong  
carbon uptake from the atmosphere. Combining the water surface area of wet season (122 days and the  
area of  $770 \text{ km}^2$ ) and dry season (243 days and the area of  $560 \text{ km}^2$ ), we estimated total  $\text{CO}_2$  efflux from  
the Yellow River source region at about  $0.37 \pm 0.49 \text{ Tg C yr}^{-1}$ , suggesting a net carbon source for the  
390 atmosphere. This efflux contrasts with the earlier estimate by Ran et al. (2015b) which reported a carbon  
sink of  $-0.168 \pm 0.084 \text{ Tg C yr}^{-1}$ .

Unlike our systematic sampling within the Yellow River source region, Ran et al. (2015b) estimated the  
riverine  $\text{CO}_2$  outgassing of the Yellow River source region by only using sampling results at five sampling  
395 sites. There are a number of reasons for the huge  $\text{CO}_2$  efflux difference. Firstly, the sampling by Ran et  
al. (2015b) was confined to the mainstream channel of the Yellow River and its major tributaries, which  
may have underestimated riverine  $\text{CO}_2$  emissions in lower-order streams. For example, our study on the  
rivers of the Zoige peatland indicated that the higher  $F\text{CO}_2$  was observed at the lower-order headstream  
tributaries (i.e.,  $767 \pm 1144 \text{ g C m}^{-2} \text{ yr}^{-1}$ ) instead of the mainstream (i.e.,  $351 \pm 306 \text{ g C m}^{-2} \text{ yr}^{-1}$ ). This is  
400 because the soil carbon-rich peatland around the rivers can be rapidly transported into the river network  
by strong physical erosion. However, with increasing flow discharge and enhanced erosion, the river  
channels are heavily cut into the bedrock, mobilization the subsurface soils with less soil carbon content  
has likely caused the dilution effect of  $p\text{CO}_2$  in the mainstream (Crawford et al., 2013). Another reason  
is that the number of sampling points limited the accuracy of  $\text{CO}_2$  emissions of relatively large watershed,  
405 especially in the alpine area and intermitted rivers. This is due to the fact that in the rivers of the source



area, the high-concentration dissolved CO<sub>2</sub> groundwater is an important source of river CO<sub>2</sub>, two groundwater samples collected in the grassland covered area showed an average  $p\text{CO}_2$  of 1976  $\mu\text{atm}$ , 2.5 times larger than that in the river (771±380  $\mu\text{atm}$ ). The CO<sub>2</sub> which originates from groundwater can be quickly released to the atmosphere within a short distance (Hotchkiss et al., 2015). In the case of point  
410 deployment, this process is difficult to monitor without the high-density sampling points arrange. Therefore, it is easy to neglect this part of CO<sub>2</sub> by representing the entire basin with relatively few sampling points.

The area of the Yellow River source region account for about 17.6% of the whole Yellow River basin and  
415 support around 4% of the total CO<sub>2</sub> efflux. Although it is still a small proportion of CO<sub>2</sub> emissions compared with the whole Yellow River Basin, but there is a huge carbon emissions potential. Since the permafrost in the source region of the Yellow River is rich in large amounts of ice and organic carbon, the continuously increasing temperature due to global warming will accelerate not only the mobilization of organic carbon in permafrost, but also the degradation of organic carbon by soil microorganisms. As  
420 a consequence, huge amounts of CO<sub>2</sub> release from soils is anticipated and relevant studies will be needed to comprehensively understand the implications of changes in riverine carbon fluxes.

Although we have made some improvements to evaluate the riverine CO<sub>2</sub> emission in the Yellow River source region, we have more accurately estimated the  $F\text{CO}_2$  by in situ measurement and discussed the  
425 riverine CO<sub>2</sub> outgassing within four land cover types, but there are still many uncertainties in our research. Firstly, despite the slight increase in sampling sites compare with the previous studies, there was less extensive research on single watersheds that are spatially representative. And in terms of time, there was a lack of continuous sampling of long sequences. Existing research suggests that the rainstorms will have



a huge shift on CO<sub>2</sub> emission (Smits et al., 2017) and we lacked the monitoring of CO<sub>2</sub> outgassing during  
430 heavy rain period. These factors caused some uncertainties of the riverine CO<sub>2</sub> evasion research and  
high frequency and long-time sequence studies under specific land cover types need to be performed in  
the future.

### 5. Conclusions

Based on four rounds of field direct measurements of CO<sub>2</sub> outgassing within the Yellow River source  
435 region, the average *p*CO<sub>2</sub> in the study area was estimated at 771±380 μatm, and the average *F*CO<sub>2</sub> was  
590±766 g C m<sup>-2</sup> yr<sup>-1</sup>. It is lower than other rivers in the world, and at a relatively low level compared to  
the middle and lower reaches of the Yellow River. The results showed that the rivers in the Yellow River  
source region were the source of CO<sub>2</sub>. Both the *p*CO<sub>2</sub> and *F*CO<sub>2</sub> showed strong spatial and temporal  
variations. The largest CO<sub>2</sub> release from rivers was found in August, followed by October and April, and  
440 the lowest was observed in June. When grouped into different land cover types, *F*CO<sub>2</sub> in the permafrost  
regions was the lowest among the four types of land cover. The highest *F*CO<sub>2</sub> was found in peatland  
river, followed by grassland and glacier region.

In alpine climates, low temperature conditions played a crucial role in limiting biological activity and  
445 reducing CO<sub>2</sub> emissions in the region. As a consequence, control both riverine CO<sub>2</sub> source and gas  
transfer velocity. The DOC has huge influence on all land cover types. In the permafrost region, the large  
amount soil related DOC could support riverine CO<sub>2</sub> concentration. In the glacier region, the glacial DOC  
and CO<sub>2</sub> may play an essential role in CO<sub>2</sub> outgassing. In the peatland and grassland region, the plants  
related DOC is an important source of riverine CO<sub>2</sub>.

450

By integrating seasonal changes of water surface area, the CO<sub>2</sub> efflux was estimated at 0.37±0.49 Tg C



yr<sup>-1</sup>, which is significantly different from the earlier estimate by Ran et al. (2015). Very few studies have focused on the dynamics of riverine carbon cycling on the Tibetan Plateau river systems. This study provides insight into the riverine CO<sub>2</sub> outgassing in the Yellow River source region, which will help better understanding of carbon emissions from alpine rivers in the world, in particular these located on the Tibetan Plateau.

**Acknowledgements:** This work was supported by the Inner Mongolia University (grant: 30150-135114), the Natural Science Foundation of China (grants: 21800-5161101).

460

#### Reference

- Abril, G., Martinez, J.M., Artigas, L. F., Moreira-Turcq, P., Benedetti, M. F., Vidal, L., Meziane, T., Kim, J.-H., Bernardes, M. C., and Savoye, N.: Amazon River carbon dioxide outgassing fueled by wetlands, *Nature*, 505, 395–398, 2014.
- 465 Alin, S. R., Maria, D. F. F. L. R., Salimon, C. I., Richey, J. E., Holtgrieve, G. W., Krusche, A. V., and Snidvongs, V.: Physical controls on carbon dioxide transfer velocity and flux in low-gradient river systems and implications for regional carbon budgets. *Journal of Geophysical Research Biogeosciences*, 116 (G1), 248–255, 2014.
- Aufdenkampe, A. K., Mayorga, E., Raymond, P. A., Melack, J. M., Doney, S. C., Alin, S. R., Aalto, R. E., and Yoo, K.: Riverine coupling of biogeochemical cycles between land, oceans, and atmosphere. *Frontiers in Ecology & the Environment*, 9 (1), 53–60, 2011.
- 470 Battin, T. J., Kaplan, L. A., Findlay, S., Hopkinson, C. S., Marti, E., Packman, A. I., Newbold, J. D., and Sabater, F.: Biophysical controls on organic carbon fluxes in fluvial networks. *Nature Geoscience*, 1 (8), 95–100, 2008.
- 475 Billett, M. F., Garnett, M. H., and Dinsmore, K. J.: Should aquatic CO<sub>2</sub>, evasion be included in contemporary carbon budgets for peatland ecosystems? *Ecosystems*, 18 (3), 471–480, 2015.
- Butman, D., and Raymond, P. A.: Significant efflux of carbon dioxide from streams and rivers in the United States, *Nature Geoscience*, 4, 839–842, 2011.
- Chang, G., Li, L., Zhu, D., Wang, Z., Xiao, J., and Li, F.: Changes and Influencing Factors of Surface Water Resources in the Source Region of the Yellow River. *Acta Geographica Sinica*, (03): 312–320, 2007.
- 480 Crawford, J. T., Striegl, R. G., Wickland, K. P., Dornblaser, M. M., and Stanley, E. H.: Emissions of



- carbon dioxide and methane from a headwater stream network of interior Alaska. *Journal of Geophysical Research Biogeosciences*, 118 (2), 482–494, 2013.
- 485 Crawford, J T., Dornblaser, M M., Stanley, E H., Clow D W., and Striegl R D.: Source limitation of carbon gas emissions in high-elevation mountain streams and lakes. *Journal of Geophysical Research Biogeosciences*, 120 (5): 952–964, 2015.
- Cole, J. J., Cole, J. J., Caraco, N. F., and Caraco, N. F.: Carbon in catchments: connecting terrestrial carbon losses with aquatic metabolism. *Marine & Freshwater Research*, 52 (1), 101–110, 2001.
- 490 Cole, J. J., Prairie, Y. T., Caraco, N. F., McDowell, W. H., Tranvik, L. J., Striegl, R. G., Duarte, C. M., Kortelainen, P., Downing, J. A., Middelburg, J. J., and Melack, J.: Plumbing the global carbon cycle: Integrating inland waters into the terrestrial carbon budget, *Ecosystems*, 10, 171–184, 2007.
- Dickson, A. G., Sabine, C. L., and Christian, J. R.: Guide to best practices for ocean CO<sub>2</sub> measurements. Pices Special Publication, 2007.
- 495 Dinsmore, K. J., M. F. Billett, and K. E. Dyson, Temperature and precipitation drive temporal variability in aquatic carbon and GHG concentrations and fluxes in a peatland catchment, *Global Change Biol.*, 19 (7), 2133–2148, 2013.
- Drake, T. W., Raymond, P. A., and Spencer, R. G.: Terrestrial carbon inputs to inland waters: A current synthesis of estimates and uncertainty, *Limnology and Oceanography Letters*, doi: 10.1002/lol2.10055, 500 2017.
- Frankignoulle, M.: Field measurement of air-sea CO<sub>2</sub> exchange. *Optik-International Journal for Light and Electron Optics*, 33 (3), 313–322, 1988.
- Hu, J.: GHG gas emissions and spatiotemporal variation from rivers in Zoige plateau, Northwest A&F University, 2015.
- 505 Hood, E., Battin, T. J., Fellman, J., O'neel, S., and Spencer, R. G.: Storage and release of organic carbon from glaciers and ice sheets, *Nature Geoscience*, 8, 91–96, 2015.
- Hood, E., Fellman J., Spencer R., Hernes P., Edwards R., Amore D., and Scoot D.: Glaciers as a source of ancient and labile organic matter to the marine environment, *Nature*, 462, 1044–1047, 2009.
- Hope, D., S. M. Palmer, M. F. Billett, and J. J. C. Dawson, Variations in dissolved CO<sub>2</sub> and CH<sub>4</sub> in a 510 first-order stream and catchment: A investigation of soil-stream linkages, *Hydrological Process.*, 18(17), 3255–3275, 2004.
- Hotchkiss, E. R., Jr, R. O. H., Sponseller, R. A., Butman, D., Klaminder, J., Laudon, H., Rosvall, M., and Karlsson.: Sources of and processes controlling CO<sub>2</sub> emissions change with the size of streams and rivers. *Nature Geoscience*, 8 (9), 2015.
- 515 Hunt, C. W., Salisbury, J. E., and Vandemark, D.: Contribution of non-carbonate anions to total alkalinity and overestimation of *p*CO<sub>2</sub> in new England and New Brunswick rivers. *Biogeosciences*, 8 (10), 3069–



- 3076, 2011.
- Humborg, C., C.-M. Mörth, M. Sundbom, H. Borg, T. Blenckner, R. Giesler, and V. Ittekkot.: CO<sub>2</sub> supersaturation along the aquatic conduit in Swedish watersheds as constrained by terrestrial respiration, aquatic respiration and weathering. *Global Change Biology*, 16 (7): 1966–1978, 2010.
- 520 Jähne, B., Heinz, G., and Dietrich, W.: Measurement of the diffusion coefficients of sparingly soluble gases in water. *Journal of Geophysical Research Oceans*, 92(C10), 10767–10776, 1987.
- Liu, S., Lu, X., Xia, X., Zhang, S., Ran, L., Yang, X., Liu, T.: Dynamic biogeochemical controls on river pCO<sub>2</sub> and recent changes under aggravating river impoundment: An example of the subtropical Yangtze
- 525 River. *Global Biogeochemical Cycles*, 30(6), 2016.
- Lorke, A., Bodmer, P., Noss, C., Alshboul, Z., Koschorreck, M., Somlai-Haase, C., Bastviken, D., Flury, S., McGinnis, D. F., Maeck, A., Müller, D., and Premke, K.: Technical note: drifting versus anchored flux chambers for measuring greenhouse gas emissions from running waters, *Biogeosciences*, 12, 7013–7024, 2015.
- 530 Lu, Z., Gao, H., Qiu, S., and Lin, Y.: The Remote Sensing Investigation and Research on Vegetation Coverage Characteristics and Environmental Impact in the Upper Reaches and Source Regions of the Yellow River. *Shanxi Environment*, 8(4):36–38, 2001.
- Marx A, Dusek J, Jankovec J, Sanda, M., Vogel, T., Geldern, R.V., Hartmann, J., and Barth, J.A.C.: A review of CO<sub>2</sub> and associated carbon dynamics in headwater streams: A global perspective. *Reviews of*
- 535 *Geophysics*, 2017, 55(2):560–585.
- Matthews, C. J., St Louis, V. L., and Hesslein, R. H.: Comparison of three techniques used to measure diffusive gas exchange from sheltered aquatic surfaces. *Environmental Science & Technology*, 37(4), 772, 2003.
- Meese, D., Gow, A., Alley, R., Zielinski, G., Grootes, P., Ram, M., Taylor, K., Mayewski, P., and Bolzan, J.: The Greenland Ice Sheet Project 2 depth-age scale: Methods and results, *Journal of Geophysical Research Oceans*, 102(C12):26411–26423, 1997.
- 540 Neal, C., W. A. House., H. P. Jarvie., and A. Eartherall.: The significance of dissolved carbon dioxide in major lowland rivers entering the North Sea, *Science of the Total Environment*, s 210–211 (1–6): 187–203, 1998.
- 545 Peter, H., Singer, G. A., Preiler, C., Chiffard, P., Steniczka, G., and Battin, T. J.: Scales and drivers of temporal pCO<sub>2</sub> dynamics in an Alpine stream, *Journal of Geophysical Research: Biogeosciences*, 119, 1078–1091, 2014.
- Ran, L., Lu, X X., Richey, J E., Sun, H., Han, J., Yu, Y., Liao, S., and Yi, Q.: Long-term spatial and temporal variation of CO<sub>2</sub> partial pressure in the Yellow River, China. *Biogeosciences*, 2015 a,
- 550 12(4):921–932.



- Ran, L., Lu, X. X., Yang, H., Li, L., Yu, R., Sun, H., and Han, J.: CO<sub>2</sub> outgassing from the Yellow River network and its implications for riverine carbon cycle. *Journal of Geophysical Research: Biogeosciences*, 2015b, 120:1334–1347.
- 555 Ran, L., Li, L., Tian, M., Yang, X., Yu, R., Zhao, J., Wang, L., Lu, X.: Riverine CO<sub>2</sub> emissions in the Wuding River catchment on the Loess Plateau: Environmental controls and dam impoundment impact. *Journal of Geophysical Research Biogeosciences*, 122 (6), 2017.
- Raymond, P. A., Hartmann, J., Lauerwald, R., Sobek, S., McDonald, C., Hoover, M., Butman, D., Striegl, R., Mayorga, E., and Humborg, C.: Global carbon dioxide emissions from inland waters, *Nature*, 503, 355–359, 2013.
- 560 Schelker J., Singer GA., Ulseth AJ., Hengsberger S., and Battin TJ.: CO<sub>2</sub> evasion from a steep, high gradient stream network: importance of seasonal and diurnal variation in aquatic *p*CO<sub>2</sub> and gas transfer. *Limnology & Oceanography*, 61:1826–38, 2016. doi:10.1002/lno.10339.
- Singer, G., Fasching, C., Wilhelm, L., Niggemann, J., Steier, P., Dittmar, T., Battin, T.: Biogeochemically diverse organic matter in Alpine glaciers and its downstream fate. *Nature Geoscience*, 5, 710–714, 2012.
- 565 Smits, A. P., Schindler, D. E., Holtgrieve, G. W., Jankowski, K. J., and French, D. W.: Watershed geomorphology interacts with precipitation to influence the magnitude and source of CO<sub>2</sub> emissions from Alaskan streams, *Journal of Geophysical Research: Biogeosciences*, 122, 1903–1921, 2017.
- Sorribas, M. V., Motta Marques, D., Castro, N. M. d. R., and Fan, F. M.: Fluvial carbon export and CO<sub>2</sub> efflux in representative nested headwater catchments of the eastern La Plata River Basin, *Hydrological Processes*, 31, 995–1006, 2017.
- 570 Stumm, W., and J. J. Morgan.: *Aquatic Chemistry: Chemical equilibria and Rates in Natural Waters*, Cram101 Textbook Outlines to Accompany, 179 (11): A277, 1996.
- Sun, W., Cheng, B., and Li, R.: Multi time Scale Correlations Between Runoff and Regional Climate Variations in the Source Region of the Yellow River. *Acta Geographica Sinica*, (01): 117–127, 2009.
- 575 Su, Z., Zhang, L., and Wang, X.: Influencing factors of partial pressure of CO<sub>2</sub> in Huanghe (Yellow River). *Marine Science*, 2005, (4): 41–44.
- Ulseth, A. J., Bertuzzo, E., Singer, G. A., Schelker, J., and Battin, T. J.: Climate-induced changes in spring snowmelt impact ecosystem metabolism and carbon fluxes in an alpine stream network, *Ecosystems*, 21, 373–390, 2018.
- 580 Waldron, S., E. M. Scott, and C. Soulsby.: Stable isotope analysis reveals lower-order river dissolved inorganic carbon pools are highly dynamic, *Environmental Science & Technology*, 41(17):6156–6162, 2007. doi:10.1021/es0706089.
- Wang, M., Liu, Z., Ma, X., and Wang, G.: Division of Organic Carbon Reserves of Peatlands in China.



- 585 Wetland Science, (2): 156–163, 2012.
- Wang, S., Sheng, Y., Gao, W., Li, J., Ma, S., Hu, Y.: Estimation of permafrost ice reserves in the source area of the Yellow River using landform classification, *Advances in Water Science*, 28 (6): 801–810, 2017.
- Weiss, R. F.: Carbon dioxide in water and seawater: the solubility of a non-ideal gas, *Marine Chemistry*, 2, 203–215, 1974.
- 590 Weyhenmeyer, G., Kosten S., Wallin, M., Tranvik, L., Jeppesen, E., and Roland, F.: Significant fraction of CO<sub>2</sub> emissions from boreal lakes derived from hydrologic inorganic carbon inputs. *Nature Geoscience*, 8(12):933–936, 2015.
- Wu, W., Xu, S., Yang, J., and Yin, H.: Silicate weathering and CO<sub>2</sub> consumption deduced from the seven Chinese rivers originating in the Qinghai-Tibet plateau. *Chemical Geology*, 249(3), 307–320, 2008.
- 595 Wu, X., Wang, N., Li, Q., Chen, L., and Jiang, X.: Ionic Compositions of Surface Snow in the Yehelong Glacier of Anyemaqen Mountains in the Headwaters of Yellow River, *Journal of Glaciology and Geocryology*, 30 (3): 415–420, 2008.
- 600 Yang, K.: Research on Characteristics of Precipitation and Runoff in the Upper Yellow River. *Gansu Electric Power*, (6): 1–14, 1991.
- Zeng, Y., Feng, Z., Cao, G., and Xue, L.: The Soil Organic Carbon Storage and Its Spatial Distribution of Alpine Grassland in the Source Region of the Yellow River. *Acta Geographica Sinica*, 59(4):497-504, 2004.
- 605 Zhang, L. J., Wang, L., Cai, W. J., Liu, D. M., and Yu, Z. G.: Impact of human activities on organic carbon transport in the yellow river. *Biogeosciences*, 10 (4), 2513–2524, 2013.
- Zhang, L., Xu, X., and Wen, Z.: Control factors of *p*CO<sub>2</sub> and CO<sub>2</sub> degassing fluxes from the Yellow River in autumn. *Advances in Water Science*, (2): 227–235, 2009.
- Zhang, Y., and Wu, Y.: Analysis of Groundwater Replenishment in the Middle Reaches of Heihe River, 610 *Journal of Desert Research*, 29 (2): 370–375, 2009.
- Zhang, Y., Zhang, S., Zhai X., and Xia, J.: Runoff Variation in the Three Rivers Source Region and Its Response to Climate Change. *Acta Geographica Sinica*, (1): 71–82, 2012.
- Zhang, Y.: The carbon flux and maintaining mechanism of *p*CO<sub>2</sub>. Ocean University of China, 2008.



Table 1. Land cover types, altitude, stream types, pH, alkalinity, DOC, pCO<sub>2</sub>, and FCO<sub>2</sub> of the 36 stream sites within the Yellow River source region, expressed in the order of April, June, August, and October.

Name	Land cover types	Apr						Jun						Aug						Oct																	
		pH	mmol L <sup>-1</sup>	mg L <sup>-1</sup>	mg L <sup>-1</sup>	DOC	pCO <sub>2</sub>	FCO <sub>2</sub>	gC m <sup>-2</sup> yr <sup>-1</sup>	pH	mmol L <sup>-1</sup>	mg L <sup>-1</sup>	mg L <sup>-1</sup>	DOC	pCO <sub>2</sub>	FCO <sub>2</sub>	gC m <sup>-2</sup> yr <sup>-1</sup>	pH	mmol L <sup>-1</sup>	mg L <sup>-1</sup>	mg L <sup>-1</sup>	DOC	pCO <sub>2</sub>	FCO <sub>2</sub>	gC m <sup>-2</sup> yr <sup>-1</sup>	pH	mmol L <sup>-1</sup>	mg L <sup>-1</sup>	mg L <sup>-1</sup>	DOC	pCO <sub>2</sub>	FCO <sub>2</sub>	gC m <sup>-2</sup> yr <sup>-1</sup>				
M1	grassland	8.4	4.4	7.4	4.6	662	435	8.6	2.5	6.4	2.5	513	224	7.5	-	6.6	4.7	758	794	8.6	2.9	8.1	-	6.43	316	8.1	-	6.43	316	8.1	-	6.43	316				
M2	glacier	8.4	3.5	8.6	5.4	550	184	8.6	1.9	7.2	3.6	483	809	7.1	-	6.6	3.5	514	212	7.3	2.3	8.2	5.4	678	199	8.2	5.4	678	199	8.2	5.4	678	199				
M3	grassland	8.5	4	7.5	3.9	525	451	8.7	3.1	6.8	9.5	572	28	7	-	6.4	3.8	715	497	7.8	3.1	-	1.3	535	374	7.8	3.1	-	1.3	535	374	7.8	3.1	-	1.3	535	374
GR1	grassland	7.9	1.7	8.6	3.7	886	307	8.2	2.1	6.6	1.2	538	184	7.6	2.4	7.1	3.6	1056	1603	7.3	1.8	7.4	1.4	830	589	7.4	1.4	830	589	7.4	1.4	830	589				
GR2	grassland	8.5	4.8	6.8	5.9	571	583	8.6	-	7.3	5.3	488	49	7.8	-	6.5	-	1095	1607	7.3	3.7	7.6	3.1	822	724	7.6	3.1	822	724	7.6	3.1	822	724				
GR3	grassland	8.2	2.8	7.1	10.0	686	297	8.2	2.1	8.6	5.1	1490	98	7.1	2.8	5.9	8.2	611	120	8	1.6	5.9	4.7	719	202	8	1.6	5.9	4.7	719	202	8	1.6	5.9	4.7	719	202
GR4	grassland	8.6	4.2	6.7	3.6	614	175	8.7	3	6.7	5.4	479	71	7	2.7	6.0	6.9	552	524	7.3	3.9	8.0	6.6	510	1361	7.3	3.9	8.0	6.6	510	1361	7.3	3.9	8.0	6.6	510	1361
GR5	grassland	8.4	4.4	7.5	-	969	1426	8.5	2.9	6.8	3.8	545	282	7.1	2.9	5.8	2.7	1197	1956	7.7	3.9	8.1	1.7	-	-	7.7	3.9	8.1	1.7	-	-	7.7	3.9	8.1	1.7	-	-
GR6	grassland	8.4	5.6	8.4	4.7	762	500	8.5	3.7	7.6	9.6	628	727	7.2	3.9	6.3	8.4	1863	1619	7.3	5.1	8.4	4.2	1084	2174	7.3	5.1	8.4	4.2	1084	2174	7.3	5.1	8.4	4.2	1084	2174
GR7	grassland	8.2	6.3	7.0	2.5	1393	889	8.2	3.2	6.5	3.0	608	438	7	3.5	6.9	2.8	2196	1478	7.2	5.5	8.2	1.7	1216	2321	7.2	5.5	8.2	1.7	1216	2321	7.2	5.5	8.2	1.7	1216	2321



GR8	grassland	8.2	2.6	8.3	7.4	720	199	8.8	1.9	9.0	7.8	478	331	7.2	2.8	7.3	2.6	1416	923	7.2	2.8	7.4	5.3	593	457
GR9	grassland	8.1	2.3	8.7	4.8	921	138	8.5	1.6	7.0	6.8	493	641	7.1	1.7	6.4	2.0	585	524	7.2	1.9	7.6	6.7	515	533
GR10	grassland	8	3.4	8.0	3.5	1124	1036	8.6	2.2	6.7	2.3	469	454	7.1	1.9	6.2	2.7	676	175	7.3	2.4	7.9	2.4	496	236
GR11	grassland	8.5	4.6	7.9	4.9	547	230	8.7	3	6.9	-	482	178	7.2	-	6.2	6.6	700	402	7.8	4.1	7.7	-	557	441
Pt1	peatland	8.6	4.8	7.3	6.3	562	448	8.6	3.4	6.0	4.5	522	107	7	3.6	6.5	2.5	1970	1358	-	3.5	7.1	5	876	1193
Pt2	peatland	8.2	5	8.5	6.3	1362	1128	8.2	3.3	8.3	3.0	598	61	7.1	1.8	6.5	6.1	1461	328	7.3	2.6	7.6	3.8	862	1251
Pt3	peatland	7.4	1	7.6	-	1809	831	7.9	-	6.6	1.4	1139	527	7.4	1.1	6.4	2.4	862	6892	8	1.2	7.4	6.8	1370	1818
Pt4	peatland	8.4	5.9	8.4	5.3	511	383	8.6	3.5	8.2	2.6	509	251	7.3	3.5	7.5	3.8	882	129	7.3	4.2	8.8	0.2	517	175
Pt5	peatland	7.7	1	7.0	5.1	576	282	8.6	1.5	7.1	7.6	660	273	7.1	1.8	6.3	4.2	523	92	7.2	1.7	7.8	4.4	856	650
Pt6	peatland	7.5	0.6	8.0	4.3	1177	1015	7.9	1.2	6.3	9.4	652	221	7.1	0.8	5.9	3.1	632	546	7.6	0.9	7.0	4.6	1206	1515
Pt7	peatland	7.6	0.7	8.2	-	612	1469	8.2	1.5	7.0	-	490	267	7.2	1.3	5.5	3.5	755	1778	7.5	1	8.0	3.2	685	123
Pt8	peatland	7.6	1.1	7.8	6.3	712	454	8.2	1.3	6.4	-	567	172	7.2	1.2	6.2	2.1	2441	1226	7.9	1.2	7.6	3.9	732	2030
Pt9	peatland	8.6	4.8	8.1	6.6	562	34	8.1	-	-	12.2	891	307	7.1	2.1	7.5	21.7	1268	61	7.3	-	7.1	5.1	1338	346
Pt10	peatland	7.8	1	7.1	5.1	865	126	8.5	1.6	-	3.0	1891	89	7.1	-	7.5	3.4	761	233	-	1.1	7.2	-	815	478
GL1	glacier	8.4	3.9	7.2	4.4	656	1190	-	-	-	-	-	-	7.6	1.2	8.3	2.1	273	-144	7.2	2.9	9.8	4.8	806	454
GL2	glacier	8.2	1.8	8.7	4.7	859	1318	8.6	-	7.5	2.0	484	83	7.5	-	6.6	-	628	392	7.5	-	7.7	-	711	399
GL3	glacier	8.5	3.1	8.2	4.7	606	156	8.7	2.3	6.8	2.8	492	52	7.3	1.9	6.4	4.5	692	583	7.8	2.5	8.0	3.9	523	230
GL4	glacier	8.4	3.1	8.1	2.7	514	205	-	-	-	-	-	-	7.5	2.1	6.6	4.5	716	328	7.8	3.1	8.4	4.6	672	328



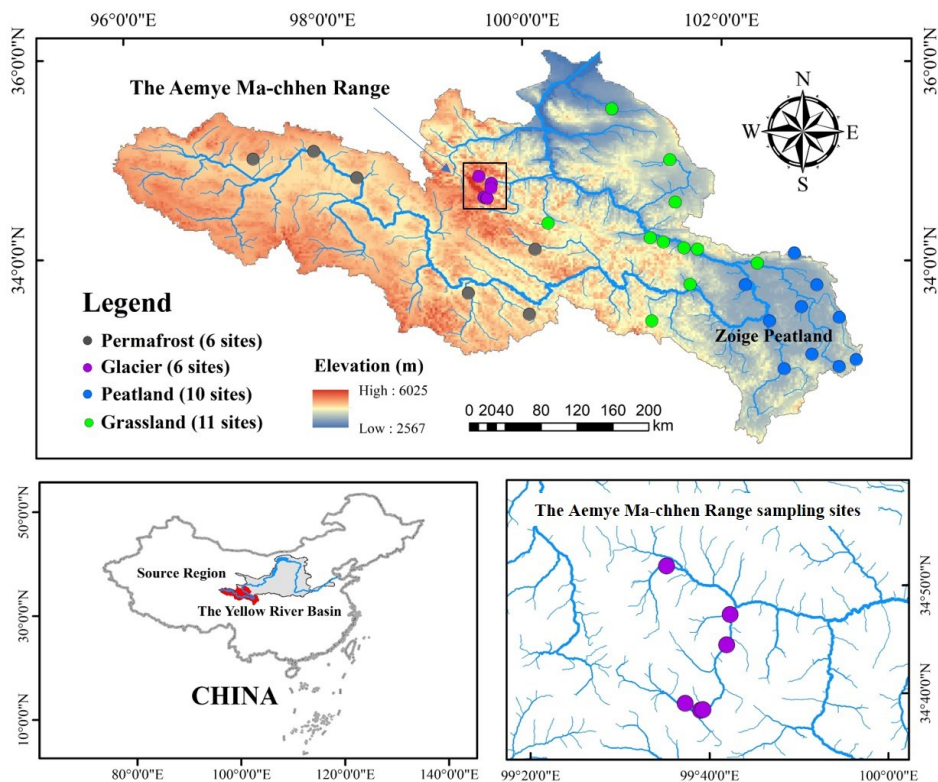


Figure 1. Sampling sites of the Yellow River Source Region

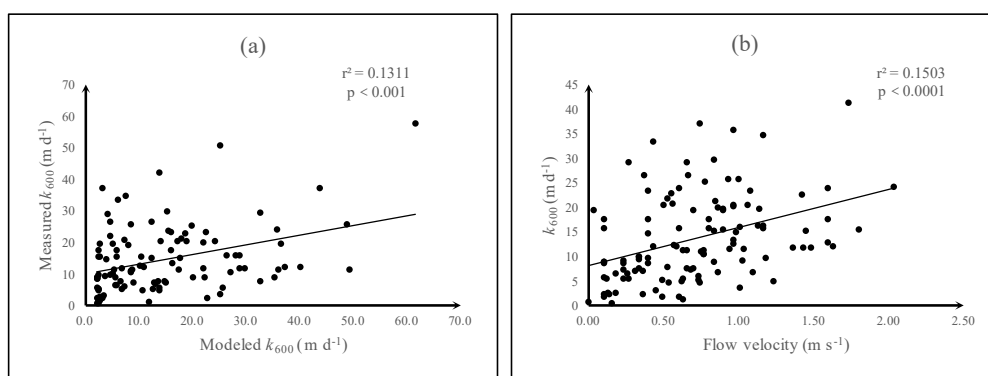


Figure 2. (a) The relationship between actual and predicted  $k_{600}$  for streams; (b) Correlation between standardized gas transfer velocity ( $k_{600}$ ) and flow velocity over the 4 campaigns. High  $k_{600}$  values ( $>70 \text{ m d}^{-1}$ ) were removed from analysis.

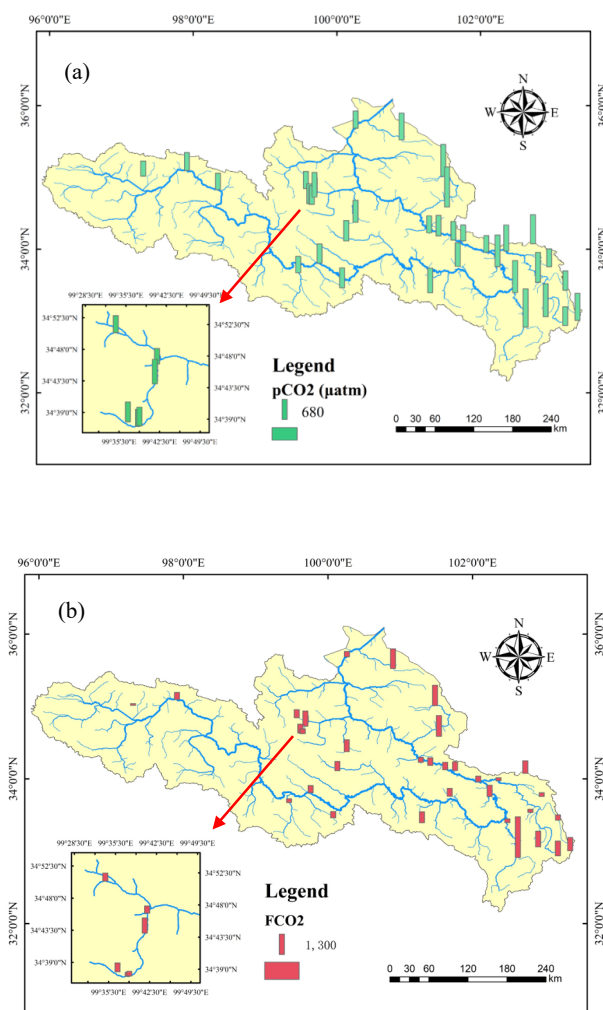


Figure 3. Spatial and temporal variations of average  $p\text{CO}_2$  (3a) and  $\text{FCO}_2$  (3b) within the Yellow River source region.

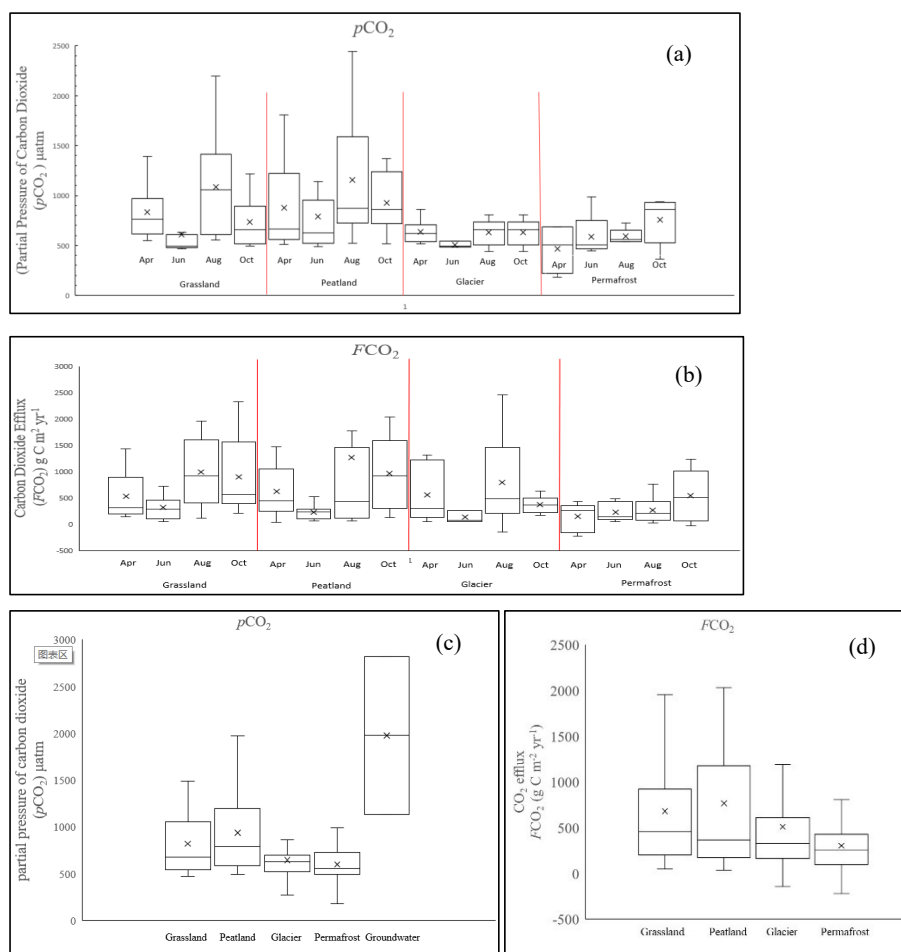


Figure 4. The box plots of  $pCO_2$  and  $FCO_2$  under four different land cover types within the Yellow River source region, expressed in the order of April, June, August, and October in Figure 4a, 4b. The  $pCO_2$  data expressed in the order of grassland, peatland, glacier, permafrost, and groundwater in figure 4c, The  $FCO_2$  expressed in the order of grassland, peatland, glacier, and groundwater in figure 4d.

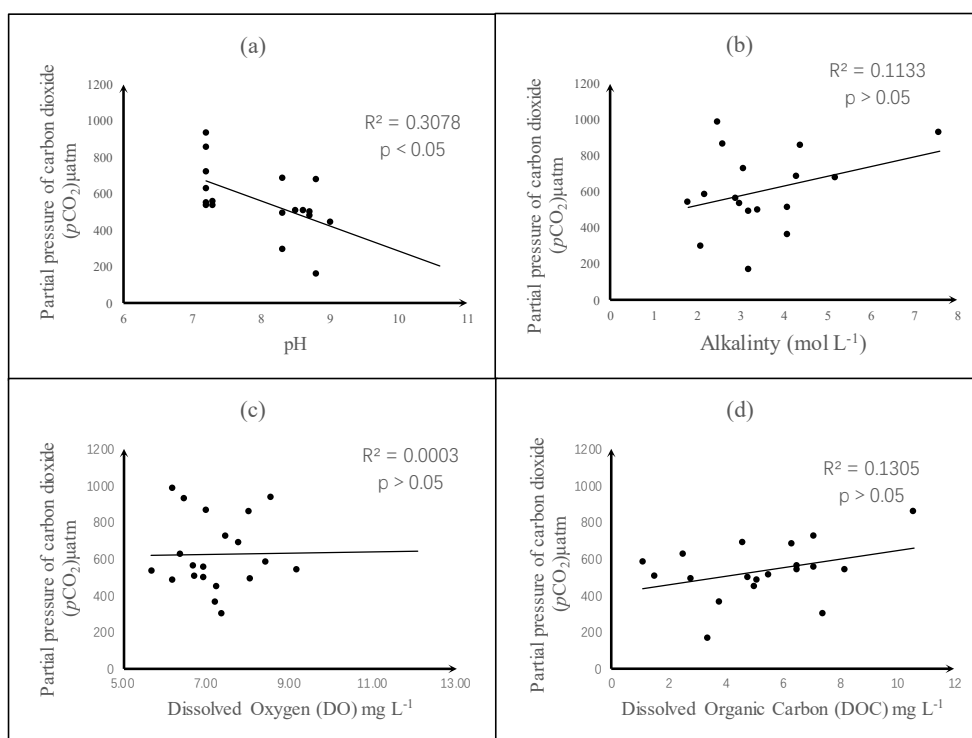


Figure 5. The linear relationship of chemical parameters and  $p\text{CO}_2$  in permafrost covered region. (a) pH, (b) alkalinity, (c) dissolved oxygen, and (d) dissolved organic carbon.

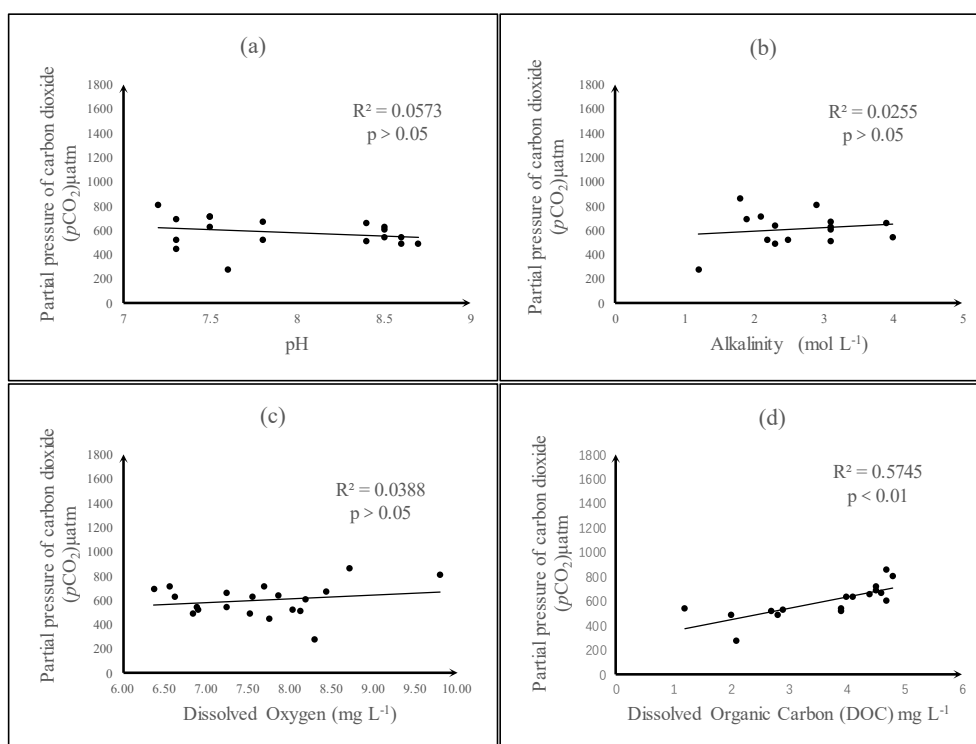


Figure 6. The linear relationship of chemical parameters and  $p\text{CO}_2$  in glacier covered region. (a) pH, (b) alkalinity, (c) dissolved oxygen, and (d) dissolved organic carbon.

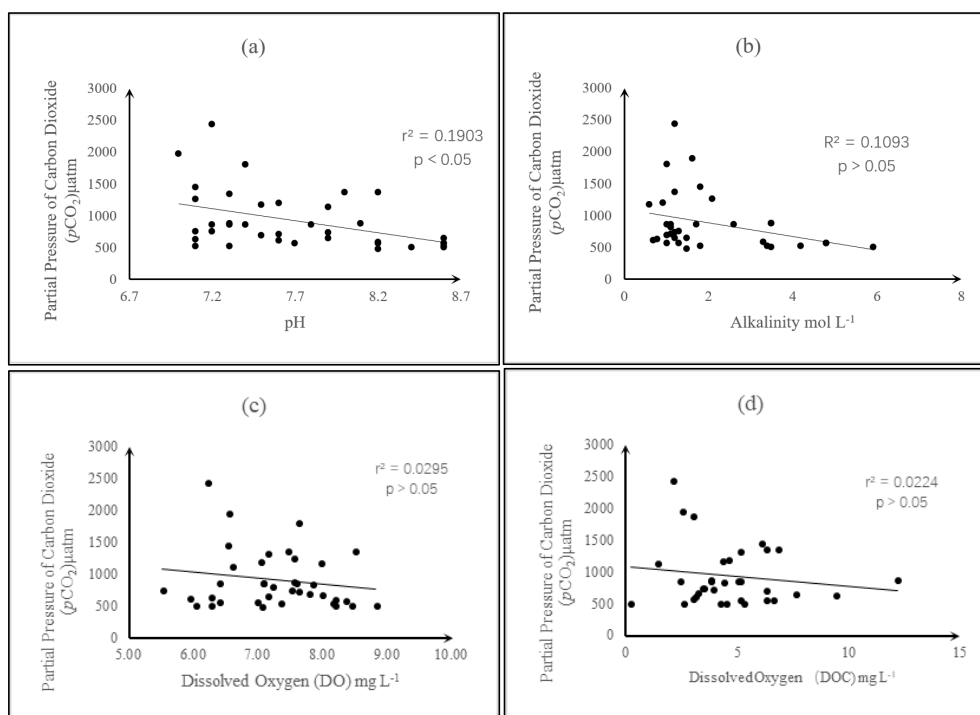


Figure 7. The linear relationship of chemical parameters and  $p\text{CO}_2$  in peatland covered region. (a) pH, (b) alkalinity, (c) dissolved oxygen, and (d) dissolved organic carbon.

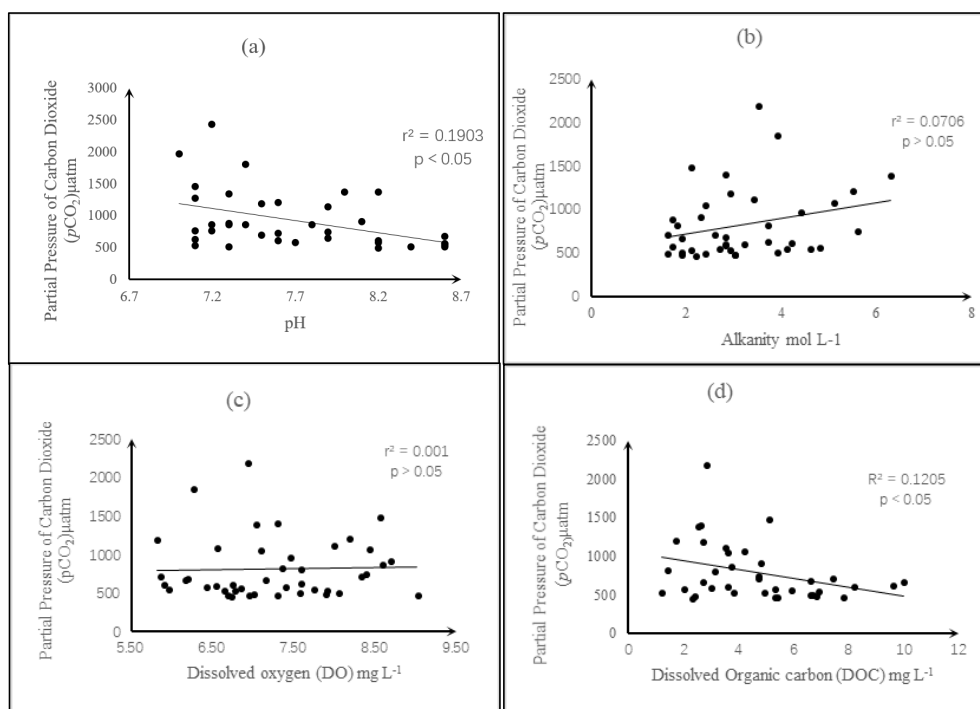


Figure 8. The linear relationship of chemical parameters and  $p\text{CO}_2$  in grassland covered region. (a) pH, (b) alkalinity, (c) dissolved oxygen, and (d) dissolved organic carbon.